Comparing Satellite and Surface Observations of Cloud Patterns in Synoptic-Scale Circulation Systems

NGAR-CHEUNG LAU AND MARK W. CRANE

Geophysical Fluid Dynamics Laboratory/NOAA, Princeton University, Princeton, New Jersey

(Manuscript received 14 October 1996, in final form 22 April 1997)

ABSTRACT

The propagation characteristics and spatial distributions of cloud cover associated with synoptic-scale circulation systems are studied using both satellite data processed by the International Satellite Cloud Climatology Project (ISCCP) and surface observations taken at weather stations or ships of opportunity. These two independent datasets produce comparable climatological patterns of the preferred direction and speed of the cloud movements. Such ''propagation vectors'' based on the ISCCP products depict cloud motions at a higher altitude than that of the corresponding movements deduced from surface synoptic reports.

By application of a similar composite procedure to the ISCCP and surface datasets, a detailed comparison is made between the satellite and surface observations of the organization of various cloud types in midlatitude cyclones. The relationships of these cloud patterns with the concurrent atmospheric circulation are illustrated by superposing the composites of wind and geopotential height on the cloud data. Both the satellite and surface observations yield well-defined cloud patterns organized about frontal zones. These cloud patterns are consistent with the composite distributions of weather types as coded in the surface reports. Combination of findings from the surface reports (which provide information on the altitude of the cloud base) and those from the satellite observations (which offer estimates of cloud-top heights) is found to be helpful for portraying the vertical distribution of cloud cover in various sectors of the extratropical cyclones. The ISCCP dataset underestimates the amount of low stratiform clouds lying under the high, optically thick cloud shield in the warm sector. Comparison between the composite results for cyclones occurring over the North Atlantic and those over the North American continent indicates the occurrence of larger anomalous cloud amounts in the continental systems. The more widespread cover by nimbostratus cloud in the northwestern sector of the surface low pressure center over land is particularly noteworthy. The distinction between the cloud organization in maritime and continental cyclones is seen to be related to the stronger, frictionally induced cross-isobaric flow over land surfaces.

Analogous composite charts are constructed for the convective disturbances occurring over the tropical western Pacific by using both satellite and surface cloud observations. Some degree of consistency is again discernible among the cloud patterns based on the two datasets. The ISCCP data tend to underestimate the amount of cumulus clouds situated below the anvils at the trailing end of these convective systems.

1. Introduction

In a recent article published in *Monthly Weather Review*, Lau and Crane (1995, hereafter referred to as LC95) examined the fluctuations of cloud properties associated with the passage of synoptic-scale circulation systems in middle and low latitudes. The daily cloud observations used in that study were derived from satellite measurements processed by the International Satellite Cloud Climatology Project [ISCCP; see reviews by Schiffer and Rossow (1983) and Rossow and Schiffer (1991)]. The typical spatial distribution of cloud types with various optical and cloud-top characteristics during prominent synoptic episodes was described in LC95 by compositing selected parameters in the ISCCP dataset. By overlaying these satellite-derived cloud fields on composites of the contemporaneous atmospheric structure, well-known relationships between the cloud and atmospheric circulation patterns have been confirmed. In the region of enhanced storm activity over the North Atlantic during winter, the representative cloud pattern as deduced from our quantitative analysis of the ISCCP data bears a considerable resemblance to that associated with typical midlatitude cyclones as reported in other synoptic studies. Over the western tropical Pacific, the summertime cloud distribution based on satellite observations is in broad agreement with that observed previously in tropical convective disturbances.

The evidence presented in LC95 illustrates the usefulness of satellite data for delineating various facets of the atmospheric circulation. The credibility of these satellite-based findings would be enhanced by verification against results derived from other observational methods. An obvious alternative to the satellite datasets is the cloud observations taken from ships and surface

Corresponding author address: Dr. Ngar-Cheung Lau, GFDL/NOAA, Princeton University, P.O. Box 308, Princeton, NJ 08542.
E-mail: gl@gfdl.gov

weather stations. An extensive effort to compile the worldwide, surface-based synoptic records of cloud type and cloud amount for the recent decades has been undertaken by Hahn et al. (1994). The primary objective of the present study is to analyze the cloud observations from sea or ground level by following essentially the same procedures developed in LC95, and to compare the results thus obtained with their counterparts based on the ISCCP dataset. In addition to cross-checking the inferences on cloud organization as drawn from two independent data sources, it is also our intention to explore the extent to which the ''top-down'' view of the cloud systems from spaceborne instruments may be augmented by the ''bottom-up'' perspective of these systems from surface observers. Our emphasis is placed on the propagation and spatial patterns of various cloud types in those regions of the northern extratropics and Tropics where synoptic-scale disturbances (i.e., phenomena with timescales of several days) are particularly active.

A brief description of the datasets and data processing procedures used in this study is given in section 2. The typical shape and propagation characteristics of the cloud patterns associated with midlatitude circulation systems are examined in section 3. Satellite- and surface-based composite cloud patterns accompanying extratropical cyclones are compared in section 4, and contrasts between maritime and continental weather systems are highlighted. Results on the cloud distributions for tropical disturbances are presented in section 5 using both ISCCP and surface data. Some discussion of the findings of this study is then made in the concluding section.

2. Datasets and analysis procedures

The present study makes use of the satellite products in the C1 dataset produced by ISCCP for the 1983–90 period. In particular, the daily averaged variations of total cloud optical thickness τ and fractional cover by different cloud types at individual grid points are analyzed. The cloud types are classified according to various thresholds of cloud-top altitude and τ (see Table 1 of LC95). Clouds with tops in the upper, middle, and lower troposphere are identified as ''high-top,'' ''middle-top,'' and ''low-top,'' respectively. Clouds with large, moderate, and small values of τ are referred to as ''thick,'' ''medium,'' and ''thin,'' respectively. Each cloud type is named by using a combination of the cloud top and τ attributes (e.g., high-top/thick, low-top/thin, etc.).

Information on the structure of the atmospheric circulation is obtained from the daily averaged gridded analyses of wind and geopotential height for the same period. These global meteorological fields are produced by the European Centre for Medium-Range Weather Forecasts (ECMWF). A detailed documentation of this dataset has been compiled by Trenberth (1992).

Surface observations of cloud types and cloud amounts are based on the synoptic cloud reports processed and edited by Hahn et al. (1994). This dataset consists of 124 million reports from land stations and 15 million reports from ships over the globe, and covers the decade from 1982 through 1991. Each report contains information on the time and location of the observation, total cloud cover, type and fraction of cloud cover at low, middle, and high altitudes, as well as a code indicating the present weather. Other supplementary variables such as cloud-base altitude are also included in the report.

To facilitate comparison between the surface observations and the ISCCP dataset, an elaborate processing scheme has been applied to the synoptic cloud reports. The details of this data analysis procedure are described in the appendix. For a given set of M selected synoptic cases, this procedure yields the composite patterns for the amount of individual cloud types ct and the frequency of occurrence of individual weather types wt on a 2.5° (latitude) by 2.5° (longitude) grid mesh. The cloud types being examined include various cumuliform and stratiform clouds with bases at low, middle, and high levels. The weather types include fog, heavy and light rain, and heavy and light snow. The composite data are expressed as anomalous departures from the long-term climatology for the corresponding season and are denoted as ANOM_{ct} and ANOM_{wt}, for a given cloud type and weather type, respectively. Hence the spatial distributions of ANOM_{ct} and ANOM_{wt} correspond to the anomalous cloud and weather patterns, which are representative of the M cases under consideration.

3. Propagation characteristics of extratropical cloud fluctuations

To gain some appreciation of the typical shape and temporal evolution of midlatitude cloud patterns as viewed from the surface, we first examine the composite anomalous distribution of the total cloud cover accompanying cloudy episodes detected in the western North Atlantic. For ease of comparison with the satellite-based results, the dates of occurrence of these episodes are exactly the same as the set of key dates used in LC95. As explained in our earlier study, these dates correspond to notable maxima in the time series of day-to-day fluctuations of cloud optical thickness τ in the ISCCP dataset for the reference site 46°N, 46°W. Nine such dates are selected in each of the seven cool seasons, so that the total number of cases M incorporated in the present composite procedure is $9 \times 7 = 63$. The anomalous composite pattern (i.e., ANOM as defined in the appendix) of surface observations of total cloud cover based on the key dates (day 0) is shown in Fig. 1b. The corresponding patterns based on data for the day before (day -1) and the day after (day $+1$) the key dates are presented in Figs. 1a and 1c, respectively. The location

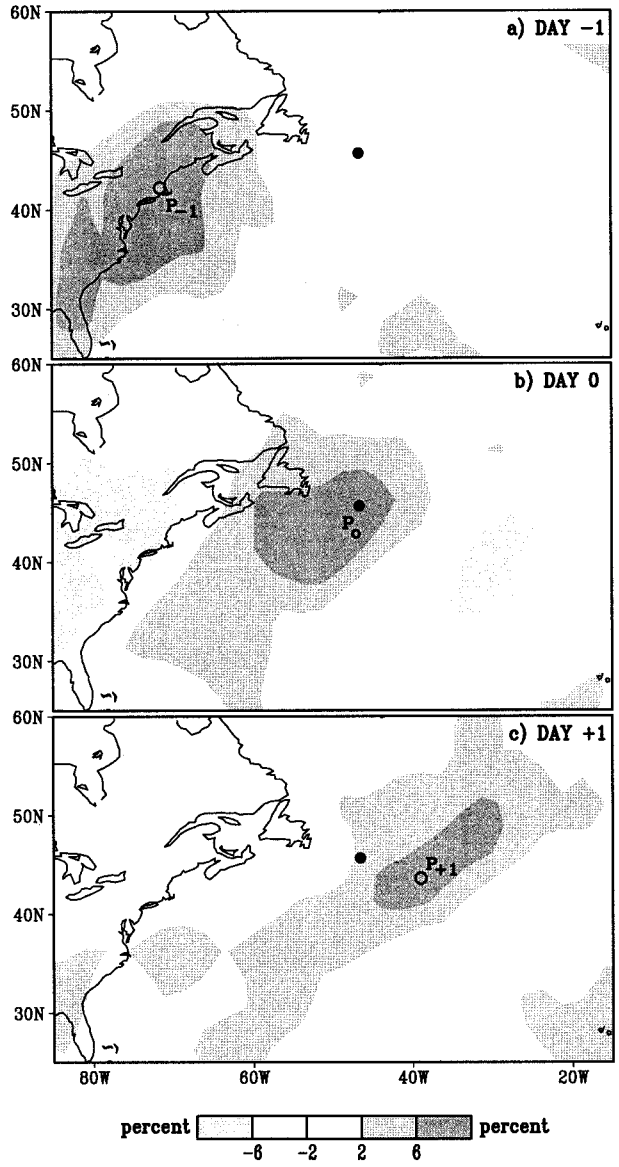

FIG. 1. Composite patterns of the anomalous total cloud amount (in percent, see scale bar at bottom) based on prominent cloudy episodes during the cool season at the reference site 46°N, 46°W. Panels (a), (b), and (c) depict the cloud distributions on the day before the key dates, the key dates, and the day after the key dates, respectively. The location of the reference site is indicated by a solid dot in each panel and is labeled as P_0 in (b). The positive extrema in (a) and (c) are indicated by open circles and are labeled as P_{-1} and P_{+1}, respectively. All patterns have been smoothed using the nine-point spatial filter described by Holloway (1958).

of the reference site P_0 is indicated as a solid dot in each panel.

It is evident from Fig. 1 that prominent cloudy events at P_0 are linked to a well-organized pattern of total cloud cover over eastern North America as well as the western and central North Atlantic. The distribution on day 0 (Fig. 1b) is indicative of a wavelike phenomenon, with enhanced cloud cover along an elongated band in the vicinity of P_0, and reduced cloud cover along similar bands farther east and farther west. The typical wavelength of this system, as estimated from the distance between the two principal bands of negative anomalies in cloud cover in Fig. 1b, is approximately 5000 km. These individual bands of cloud anomaly exhibit a characteristic orientation from the southwest to the northeast. Comparison among the three panels in Fig. 1 reveals a distinct tendency of the system of bands to migrate east-northeastward with time, at a speed of approximately 15 m s^{-1}. The above spatial and temporal characteristics of the composite charts in Fig. 1 based on surface observations are in general agreement with the corresponding patterns in Figs. 3a–c in LC95 based on satellite measurements of τ.

For a given reference site P_0, the temporal evolution of the composite cloud pattern may be depicted by a propagation vector computed using the following method. The mean locations of the principal anomaly of enhanced cloud cover one day before and one day after the key dates are estimated by noting the positive extrema appearing in the composite maps for day -1 and day $+1$ (see open circles labeled as P_{-1} and P_{+1} in Figs. 1a and 1c, respectively). The direction of the propagation vector is determined by the orientation of the line segment pointing from P_{-1} to P_{+1}. The migration speed is obtained by dividing the distance between P_{-1} and P_{+1} by 2 days. The propagation ''arrow'' thus computed is then assigned to the reference point P_0. The computation of the composite patterns and propagation arrows is repeated multiple times by successively treating individual grid boxes situated between 25° and 60°N as the reference site.

The wintertime distributions of the propagation vectors as determined by the above procedure are displayed in Fig. 2. Arrows based on the surface observations of total cloud cover are shown in red. The corresponding vectors obtained from analysis of the ISCCP data for τ (as presented in Fig. 4a of LC95) are reproduced in Fig. 2 using black arrows. Red and black arrows are plotted only in grid boxes for which the sum of the composite cloud cover anomaly at P_{-1} and at P_{+1} (which is a measure of the ''temporal coherence'' of the migratory signal during the 2-day periods centered on the key dates) exceeds 16%. Arrows are not plotted over grid points with propagations speeds less than 2 m s^{-1}. The sparsity of propagation vectors over the eastern oceans may partially be attributed to the prevalence of persistent and extensive stratus decks in those regions (Warren et al. 1988), which makes it difficult to discern day-to-day cloud movements by using surface reports.

Some of the characteristics of the propagation vectors in Fig. 2 are related to the local mean wind circulation at the altitudes where the clouds are detected. For instance, the systematic counterclockwise turning of the vectors as they go eastward from East Asia to the western North Pacific is consistent with the occurrence of a wintertime stationary trough in that region. The mag-

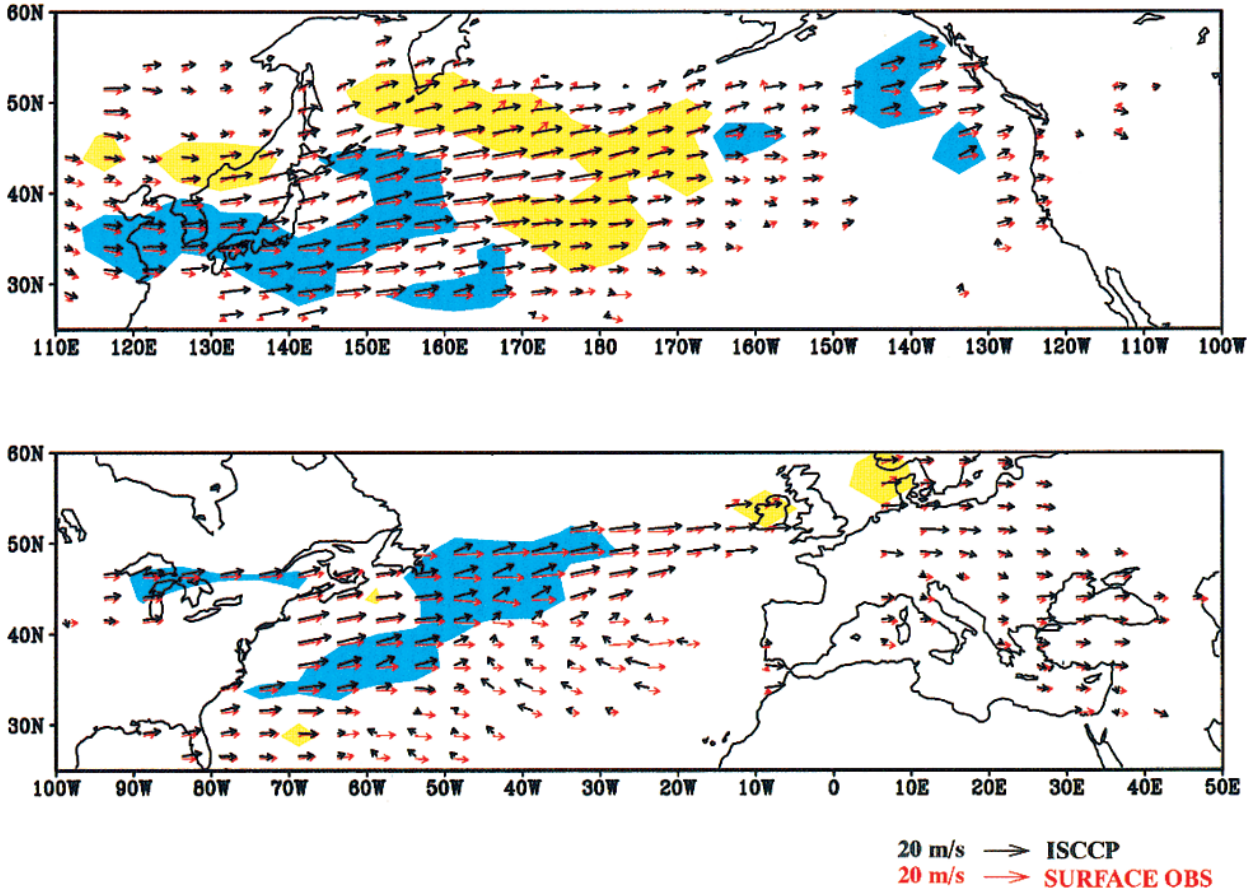

FIG. 2. Distributions of the propagation vectors during the cool season, as computed using the ISCCP data for cloud optical thickness (black arrows) and surface synoptic reports of total cloud cover (red arrows). The scaling for these arrow patterns is given at the bottom right of the figure. The zonal and meridional components of the vectors have been smoothed using the nine-point spatial filter described by Holloway (1958). Yellow (blue) shading indicates regions where the vectors based on ISCCP observations are rotated in a clockwise (counterclockwise) fashion relative to the vectors based on surface observations by more than 5°. The angular deviation between the results for satellite and surface data at a given grid point is determined only when the propagation speed for both results exceed 8 m s^{-1}.

nitude and orientation of the arrows in Fig. 2 are similar to those of the climatological wind vectors at 700 or 850 mb (e.g., see Fig. 2 of Blackmon et al. 1984).

At those sites where wavelike disturbances are active, such as the cyclone tracks within the 40°–50°N zone in the central North Pacific and North Atlantic (e.g., see Blackmon et al. 1977), the arrows in Fig. 2 may alternatively be interpreted as portraying the phase propagation of these disturbances. The association between the temporal evolution of cloud cover and movement of cyclone-scale waves is substantiated by the resemblance between the vector fields in Fig. 2 and the phase propagation patterns based on time-filtered data of geopotential height [see Fig. 2 of Blackmon et al. (1984) and Fig. 8 of Wallace et al. (1988)].

Along the axes of the jet streams over the western North Pacific (near 35°N, 120°–170°E), the propagation speed deduced from surface observations (red arrows in Fig. 2) is noticeably slower than that obtained using ISCCP data (black arrows). Similar differences are also discernible in a more limited area in the western North Atlantic (30°–40°N, near 70°W). This discrepancy could in part be attributed to the different vantage points of the surface observers and satellite platforms. For a specific location at a given time, surface-based data tend to describe characteristics of clouds that are situated at lower altitudes than those detected by satellite sensors. Since the jet stream regions are characterized by rapid increases in the local wind speed with height, the surface synoptic reports would yield comparatively slower propagation speeds.

In the jet stream regions over the western oceans, the propagation arrows based on satellite data are rotated in a counterclockwise sense relative to the arrows computed using surface data. In particular, blue shading in Fig. 2 depicts those areas where this counterclockwise rotation exceeds 5°. If we again assume that the altitude of the wind field as inferred from surface reports is typically lower than that based on ISCCP data, the differences in the orientation of the two sets of vectors

would imply a backing of the prevalent winds with height in vicinity of the jet streams. Such a vertical profile of the thermal wind is indicative of the occurrence of cold temperature advection in these regions. This inference is consistent with the climatological charts of temperature advection as presented by Lau (1979, Figs. 18a and 20a).

In the North Pacific region in 45°–50°N, 150°E–170°W, the propagation arrows based on ISCCP observations are directed mostly from west to east, whereas the corresponding arrows for the surface dataset are oriented from southwest to northeast. Yellow shading is used in Fig. 2 to highlight those regions where the arrows for the satellite data exhibit a clockwise rotation relative to the arrows for the surface data by more than 5°. The angular deviation between the two sets of arrows in this region may in part be due to differences in the direction of phase propagation of cyclone waves along the Pacific storm track at various altitudes. The vertical dependence of the propagation characteristics of synoptic-scale fluctuations may be discerned from the results presented by Blackmon (1976, Fig. 5), Blackmon et al. (1977, Fig. 2b) and Wallace et al. (1988, Fig. 8) based on time-filtered geopotential height data at different pressure levels. These findings are consistent with the tendency for surface lows (as would be preferentially sampled by cloud reports taken at the surface) to migrate poleward as they evolve through the occlusion and decay phases over the central North Pacific. In this stage of the cyclone development, the upper-level waves (as seen by the satellite instruments from above) are often decoupled from the surface disturbances and continue to travel eastward.

In the North Atlantic region from 25° to 40°N, and from 20° to 50°W, there are notable discrepancies between the propagation vectors based on ISCCP and surface reports. Differences are also seen at scattered grid points in the subtropical central and eastern Pacific. The climatological circulations in these regions are dominated by subtropical anticyclones, which are associated with much weaker wind speeds and storm intensity, and with extensive stratiform cloud cover near the boundary layer. The weak steering currents and long-lived maritime stratus decks in these regions lead to considerable uncertainties in the estimation of cloud propagation characteristics using both datasets.

4. Cloud patterns accompanying extratropical cyclones

We proceed to compare the satellite and surface views of the typical distribution of various cloud types associated with midlatitude disturbances. The ISCCP and surface datasets are subjected to essentially the same composite procedure described in section 5a of LC95. For each point in a given array of 20 reference sites, a set of 63 key dates are selected by identifying the maxima in the daily time series of cloud optical thickness τ for that point. Composites are then constructed by averaging the pertinent ISCCP, ECWMF, and surface cloud data over the key dates. Anomalies are computed by subtracting the corresponding climatological means for the northern cool season (October through March) from the composites. In our previous study, the anomalies for a given key date were defined as departures from the average over the 5-day period centered on that key date. For a given parameter, the set of 20 anomalous composite patterns thus obtained (one for each reference site in the array) is combined to form a single chart by aligning the composite data to a common Cartesian coordinate system, so that the origin of this system coincides with the reference site for each of the 20 composite patterns. The composite procedure in this study entails considerable averaging in both time and space. No attempt is made to distinguish the cloud patterns occurring in various stages of the cyclone development. These limitations should be borne in mind when comparing our results with other studies based on individual synoptic cases.

For the ISCCP data, the amount of a given cloud type is determined by taking the ratio of the number of pixels satisfying the cloud-top altitude–τ criteria for the cloud type in question versus the total number of pixels available for analysis in each grid box on each day. This ratio may be viewed as a spatial measure of the fraction of the sky covered by a particular cloud type. All subsequent computations of the composite and climatological patterns are then performed using the daily grids of these ratios. Hence the ISCCP cloud amounts correspond to temporal averages of fractions of spatial cloud cover for individual days. On the other hand, the cloud amount based on the surface data [see Eq. (A1)] is defined as the product of the frequency of occurrence of a certain cloud type (which is essentially a temporal measure) and the average fraction of cover by that cloud type whenever it is present (a spatial measure). In comparing the products from ISCCP and the surface reports, one must bear in mind the different procedures used in estimating the cloud amount from the two datasets.

a. Maritime systems

We first examine the cloud and circulation patterns accompanying the maritime disturbances over the North Atlantic. The composite results to be presented here are based on the same network of 20 reference sites used previously by LC95 (see solid dots in Fig. 5a of that paper). This staggered array of ocean points is situated east of Nova Scotia and Newfoundland and covers the region of 41°–51°N, 34°–59°W. The separation between neighboring points in this array is 5° of longitude and 2.5° of latitude. This array is situated in a region characterized by climatological cold-air advection (see section 3) and frequent cyclogenesis. The spatial patterns of the anomalous amounts of selected cloud types from the ISCCP dataset (left panels) and the surface reports

(right panels) are shown in Fig. 3. Superposed on the patterns for each cloud type are the composite anomalies of the ECMWF analyses of the height (contours) and horizontal vector wind (arrows) fields at 1000 mb. The abscissa and ordinate of each panel represent the longitudinal and latitudinal distances, respectively, from the common origin, to which the reference sites of the 20 individual composite charts are aligned. The composite procedure has been applied to every cloud type reported in the ISCCP and surface datasets. The specific cloud types in Fig. 3 are chosen for presentation by virtue of the large anomalous amounts appearing in the composite patterns for these cloud types.

The satellite-based cloud patterns (left panels of Fig. 3) exhibit well-defined relationships with the ambient circulation field. Physical interpretation of such relationships in terms of dynamical forcing and three-dimensional cyclone structure has been offered in LC95. The most prominent feature in the region east of the surface low pressure center and west of the high center (i.e., the ''warm sector,'' with predominately southerly flow) is a cloud shield that is optically thick and has a high top (Fig. 3a). Near the eastern fringe of this shield are high-top elements with lower τ (Fig. 3b). The cloud cover in the cold sector to the west of the surface low, where northerly flow prevails, consists mainly of low-top/thick clouds (Fig. 3c), and, to a lesser extent, low-top/thin clouds (Fig. 3d).

The surface synoptic reports (right panels of Fig. 3) also reveal a systematic organization of the cloud types in various sectors of the composite cyclone. The occurrence of nimbostratus (Fig. 3e) is enhanced in a broad region extending westward from the warm sector all the way to the west of low center. The maximum enhancement occurs to the east of the low and reaches an amplitude of more than 10%. Assuming that these precipitating nimbostratus clouds[1] are optically thick, the ISCCP composites indicate that the eastern two-thirds of the nimbostratus region (which corresponds to the warm sector of the cyclone) are mostly populated by clouds with high tops (Fig. 3a), whereas the remaining one-third to the west of the low (which corresponds to the cold sector) consists mainly of low-top clouds (Fig. 3c). The composite pattern for thick altostratus (Fig. 3f) bears some resemblance to that for high-top/medium clouds based on ISCCP data (Fig. 3b). The positive extrema in this pair of patterns are located near the eastern edge of the cloud shields depicted in the nimbostratus and high-top/thick composites. This spatial relationship implies that stratiform clouds with bases at middle levels (i.e., altostratus) and tops at high levels are prevalent along the leading edge of the deep rainclouds associated with the advancing warm front.

The composite pattern for nonprecipitating stratus clouds[2] based on the surface reports (Fig. 3g) indicates a notable increase of this cloud type in a large region extending southwestward from the warm sector. On the contrary, the ISCCP composite for the cloud category with attributes that correspond most closely to stratus (i.e., low cloud top and large optical thickness; see Fig. 3c) is characterized by a *decrease* in this cloud type in the warm sector. This discrepancy between the satellite and surface views of the low stratiform cloud may in part be due to the presence of thick or medium high-top clouds in the warm sector (see Figs. 3a,b), which shield whatever cloud decks that might exist underneath from the view of the satellite sensors. It is also conceivable that, in situations when stratus clouds and high-top/thin clouds coexist in the warm sector, the satellite retrieval algorithms might interpret the cloud field as being composed mainly of high-top/thick elements. A better agreement between Figs. 3c and 3g is found to the southwest of the low center, where the low clouds are not obscured from the satellite view by high-top clouds.

A reasonable correspondence is found between the satellite composites of low-top/thick and low-top/thin clouds (Figs. 3c,d) and the surface-based composite for the combined cumulus/nonprecipitating stratocumulus[2] categories (Fig. 3h). Enhanced occurrence of these cloud types is found in the cold sectors to the northwest of the low center and to the southeast of the high center. Included in such clouds are open cell convective elements often seen when cold air masses advance toward relatively warmer ocean surfaces.

In a recent study, J. R. Norris (1996, personal communication) documented the relationships between surface cloud observations and vertical soundings taken at selected weather ships. His results for the midlatitude North Atlantic during winter indicate that stratocumulus and cumulus occur in conjunction with cold temperature advection, whereas fair-weather or bad-weather stratus are associated with warm advection. These findings are in general agreement with the composite patterns presented in Fig. 3.

The relative abundance of, and the spatial relation-

[1] In editing the surface cloud observations, the nimbostratus category is assigned to reports with midlevel cloud type corresponding to thick altostratus or ''obscured sky,'' and with the current weather corresponding to drizzle, rain, or snow. Nimbostratus is also assumed to be present when (a) information on middle-level clouds is missing, the low-level cloud observation indicates either no cloud or bad-weather stratus, and the current weather corresponds to drizzle, rain, or snow; or (b) information on midlevel clouds is missing, the low-level cloud type is either fair-weather stratus or stratocumulus, and the weather type is rain or snow.

[2] Since some stratus (St) or stratocumulus (Sc) clouds are reclassified as nimbostratus clouds when the current weather indicates drizzle, rain, or snow (see footnote 1 for details), only those St or Sc reports in nonprecipitating weather situations are incorporated in these two cloud categories. There is, hence, no overlap between the reports contributing to the nimbostratus composite and the reports contributing to the St or Sc composites.

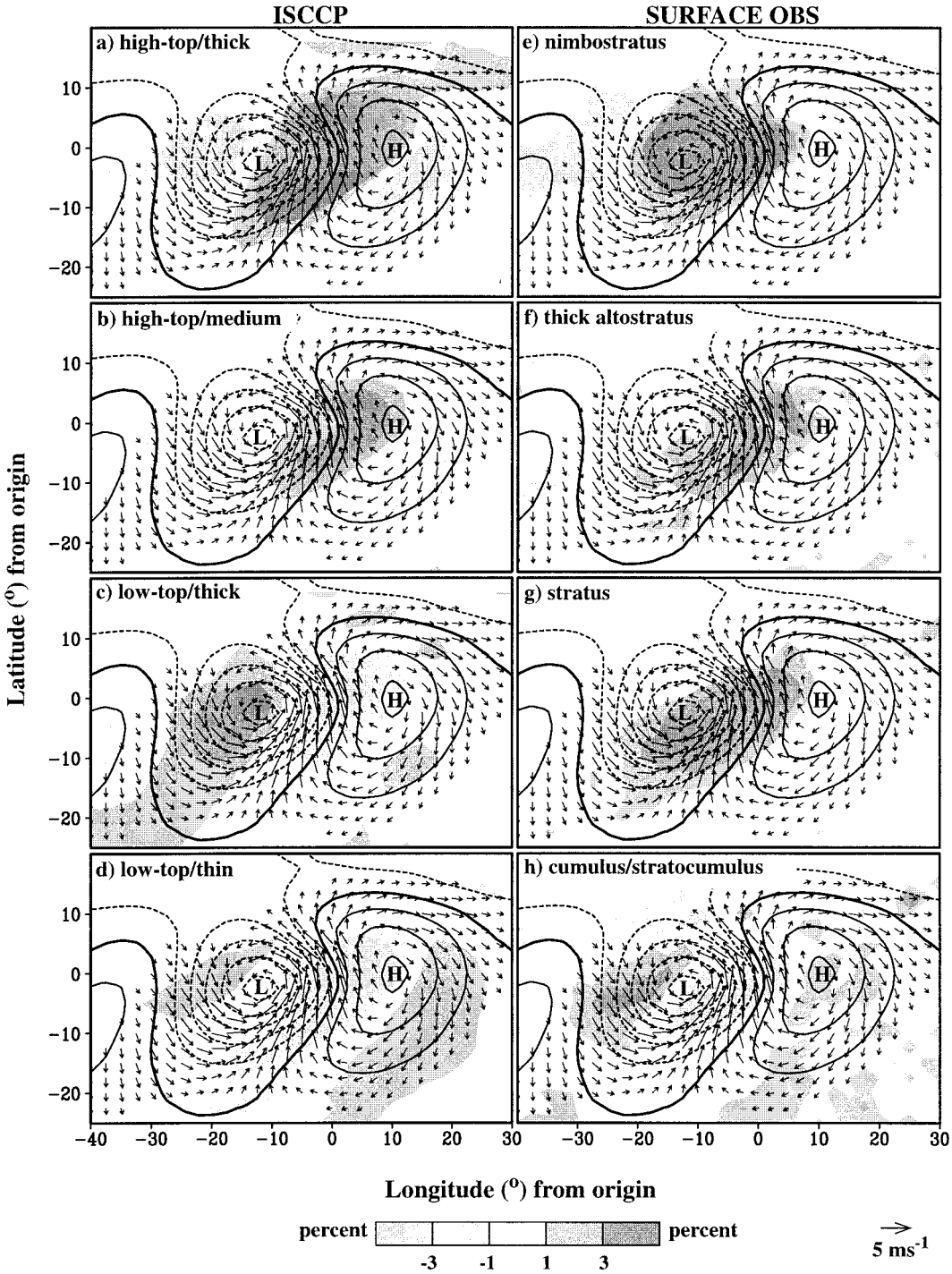

FIG. 3. Composite patterns of anomalous amounts (in percent, see stippling in each panel and scale bar at bottom) of (a) high-top/thick, (b) high-top/medium, (c) low-top/thick, and (d) low-top/thin clouds based on the ISCCP dataset, and of (e) nimbostratus, (f) thick altostratus, (g) stratus, and (h) cumulus/stratocumulus based on the surface synoptic reports. Superposed on each panel are the corresponding composites of anomalous horizontal wind vector (arrows, see scale at bottom right) and geopotential height (contours; interval: 10 m) at 1000 mb, as obtained from ECMWF analyses. Solid (dashed) contours indicate positive (negative) values. The composite procedure is based on 20 reference sites in the North Atlantic during the cool season. The ordinate (abscissa) of each panel represents latitudinal (longitudinal) displacements from the common origin, to which the composite charts for individual reference sites are aligned.

ships between the individual cloud categories considered in Fig. 3 may be discerned more easily by presenting the composite data for all cloud types in a single chart, as is done in Fig. 4 for (a) ISCCP data and (b) surface observations. Each 2.5° × 2.5° grid box in the common coordinate system used here is divided into 25 square pixels. For each cloud type being considered, the pixels are filled in a randomized fashion with a color assigned to that cloud type. The number of pixels in a grid box to be color-filled is determined according to the magnitude of the positive composite anomaly in that cloud type at that grid box: one pixel is filled for each percent of cloud amount enhancement. Negative composite anomalies are not indicated in these plots. Any unfilled pixels are indicated in black. Note that the colors used to represent these four cloud types are different from those used in LC95. As in Fig. 3, the composite anomalies in 1000-mb height and horizontal wind are superposed on the pixel patterns in Figs. 4a and 4b using contours and arrows, respectively.

The color mosaics in Figs. 4a and 4b illustrate further the similarities and differences between the cloud patterns based on the ISCCP and surface datasets as noted previously in Fig. 3. The satellite pattern (Fig. 4a) indicates a clear demarcation between high-top clouds (red and green pixels) in the warm sector and the low-top clouds (yellow and blue pixels) in the cold sector. On the other hand, the surface observers (Fig. 4b) report much larger amounts of stratus in the warm sector, so that the cloud cover in the latter region is characterized by a more heterogeneous mix of cloud types. Also evident from Figs. 4a and 4b is the collocation of the nimbostratus clouds north and west of the low center with the low-top/thick pixels in the satellite composite.

To delineate the relationships between the cloud patterns and the surface weather, the composite chart of the anomalous frequency of occurrence of four selected weather types (see definition of $\mathrm{ANOM}_{\mathrm{wt}}$ in the appendix) is shown in Fig. 4c. The plotting procedure for this diagram is analogous to that for Figs. 4a and 4b. The 25 pixels within each grid box in the common coordinate system are filled by the colors representing individual weather types wt at the rate of one pixel per each percent increase in the frequency of occurrence of each wt. Superposed on this pixel pattern is the composite anomalous pattern of 500-mb vertical velocity, $-\omega$ (see contours), as provided in the ECMWF dataset. Reports of light snow spread over an extensive region in the northwestern quadrant of the plotting domain. This weather type is not depicted in Fig. 4c (and Fig. 5c in section 4b) for the sake of clarity.

The pattern in Fig. 4c is consistent with the weather accompanying a typical midlatitude cyclone, with rain occurring in the vicinity of the warm and cold fronts, and snow to the north and west of these frontal zones. The fog reports are mostly situated along the eastern edge of the rainy region. The area of enhanced occurrence of precipitation is well collocated with the maximum in anomalous upward velocity at 500 mb. The centers of anomalous descent are almost void of any reports of precipitating weather. The good agreement between the contour and pixel patterns in Fig. 4c, which are based on entirely independent data sources, affirms the validity of the analysis procedures adopted in the present study, and also demonstrates the reliability of ECMWF estimates of the vertical velocity field in midlatitudes.

Comparison among the three panels in Fig. 4 reveals a close correspondence between precipitation reports in Fig. 4c and occurrence of nimbostratus in Fig. 4b, as can be expected from the definition of the nimbostratus cloud category (see footnote 1). It is also evident from Figs. 4a and 4c that much of the rain in the warm sector is coincident with high-top clouds, and the snowfall to the northwest of the surface low is mostly associated with clouds with low tops. The centroid of the high-top cloud shield in Fig. 4a is shifted eastward of the centers of precipitation and ascent Fig. 4c by approximately 5° of longitude. This relationship is consistent with the synoptic experience that high clouds tend to occur in advance of the precipitation during the passage of an extratropical cyclone. The spatial shift of the cloud cover relative to the center of maximum ascent is the result of eastward advection of the high cloud elements by the upper-level jet stream.

In summary, the satellite and surface observations offer complementary views of the cloud organization in a typical midlatitude cyclone. By inferring the altitudes of the base and top of the prevalent clouds from the surface reports and ISCCP data, respectively, it is feasible to estimate the vertical characteristics of the cloud cover in certain parts of the cyclone. For instance, the coincidence of surface reports of nimbostratus and stratus with mostly high-top satellite cloud pixels in the warm sector is indicative of the existence of either a deep cloud layer or multiple cloud decks. On the other hand, the collocation of nimbostratus with low-top satellite pixels in the northwestern quadrant of the low pressure area implies a much shallower cloud cover in that region. This comparative study also suggests that a one-to-one correspondence does not always exist between the cloud types identified in the ISCCP dataset (based on cloud-top height and τ) and the cloud types used in surface synoptic reports (based on visual appearance and cloud-base height). A case in point is that the nimbostratus in the warm sector can be matched with the satellite high-top/thick pixels, whereas the nimbostratus to the northwest of the low center is seen to be mostly associated with low-top/thick pixels. On the other hand, the nimbostratus cloud category has been assigned to middle-top/thick pixels in the ISCCP datasets under the classification scheme of Rossow and Schiffer (1991, see their Fig. 4). In view of these complications, caution must be exercised in associating cloud characteristics inferred from satellite measure-

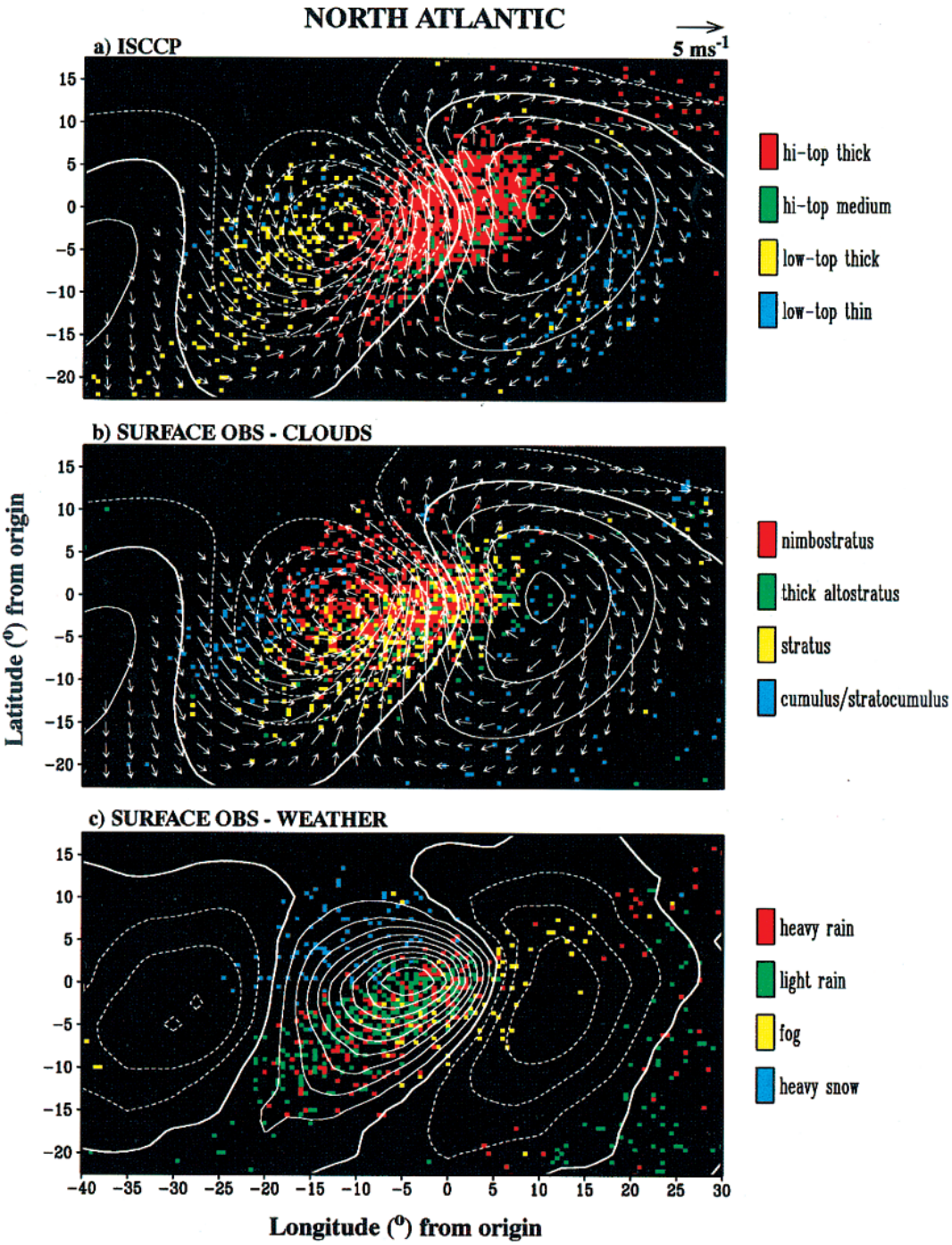

FIG. 4. Composite patterns of the positive anomalies of the amount of selected cloud types based on (a) ISCCP data and (b) surface observations, and of the (c) frequency of occurrence of selected surface weather types, for the reference sites in the North Atlantic during the cool season. The coordinate system used in each panel is identical to that used in Fig. 3. In each 2.5° × 2.5° box in this system, the presence and relative abundance of a given cloud type or weather type are depicted by plotting randomly scattered pixels with a specific color (see legends at right), at the rate of one pixel for each percent increment in cloud amount or frequency of occurrence. The arrows (see scaling at top right) and contours (interval: 10 m) in (a) and (b) indicate the composite anomalous 1000-mb wind and geopotential height fields from the ECMWF analyses, respectively. The composite anomaly pattern for the vertical velocity, $-\omega$ (with positive values indicating upward motion) from the ECMWF data is shown as contours (interval: 2×10^{-2} Pa s^{-1}) in (c). Solid (dashed) contours indicate positive (negative) values.

ments with specific morphological cloud types based on surface observations.

b. Continental systems

In order to compare the cloud organization in maritime cyclones with that occurring over land, a composite analysis of the ISCCP cloud data, surface cloud data, and surface weather reports has been repeated by using an array of 20 reference sites in the eastern half of North America. This array of land points has a similar configuration as the North Atlantic array used in section 4a, and covers the region of 36°–46°N, 74°–99°W. A set of 63 key dates is identified for each of these 20 land sites according to the times of occurrence of large τ in the time series for the site in question. These key dates are in general different from those determined for the North Atlantic sites used in section 4a. The subsequent data processing procedure is identical to that used for studying the maritime cyclones. The color mosaics thus obtained for the North American weather systems are shown in Fig. 5a for ISCCP data, Fig. 5b for surface cloud data, and Fig. 5c for surface weather type data. Superposed on the pixel patterns are the corresponding ECMWF composites of the anomalous 1000-mb height and wind fields in Figs. 5a and 5b, and the 500-mb vertical velocity in Fig. 5c.

The patterns in Figs. 5a and 5b indicate that the continental cloud shields and geopotential anomalies acquire a more isotropic character than their counterparts over the North Atlantic. In particular, the characteristic southwest-to-northeast tilt of the cloud cover and 1000-mb height anomaly seen in the maritime systems (Figs. 3 and 4) is less evident in the land systems. The less prominent horizontal tilt over North America is consistent with the weaker time-averaged meridional flux of westerly momentum by synoptic-scale eddies in that region (e.g., see Fig. 7b of Blackmon et al. 1977). These geographical differences in the eddy transport properties are related to the life cycles of eastward traveling synoptic disturbances in this region. The typical evolution of such storm systems is characterized by a baroclinic growth phase (with enhanced poleward heat fluxes) near the eastern seaboard of North America, followed by a mature phase (with enhanced eddy momentum flux convergence) farther downstream. The composite amplitude of the 1000-mb height perturbations in the continental sector is comparable to that in the oceanic sector. However, the density of color-filled cloud pixels in Figs. 5a and 5b over the continental low pressure center and in the region farther north and west is higher than that in the corresponding maritime composites (Figs. 4a and 4b). Specifically, the surface reports indicate that the enhancement of total cloud cover near the low pressure center is approximately 25% for the land composite and 10% for the ocean composite. Since the data presented here correspond to departures from climatological averages ($CLIM_{ct}$, see appendix), the larger anomalies in cloud cover over North America could in part be attributed to the lower values of $CLIM_{ct}$ over land as compared to those over maritime sites (see Warren et al. 1986, 1988).

Comparison between the satellite patterns in Figs. 4a and 5a reveals that the low-top clouds to the northwest of the continental low center are characterized by relatively larger τ. The low-top/thin clouds seen in this sector of the maritime pattern are absent from the composite in Fig. 5a. The population of low-top thick clouds to the southeast of the low pressure area is noticeably higher in the continental composite than in the maritime composite.

The surface-based composites (Figs. 4b and 5b) indicate that the nimbostratus and stratus cloud shields in the continental cyclone are extended farther to the north and to the west than their counterparts in the maritime composite. The diminished cloud cover to the northwest of the low center in the maritime pattern could in part be related to the sparsity of surface observations in that particular quadrant, which corresponds approximately to the Labrador Peninsula and the surrounding waters. The density of cumulus/stratocumulus clouds in the southeastern quadrant of the continental low pressure area is considerably higher than that in the maritime pattern. The high pressure center in the land composite is almost void of any cloud cover, in contrast to the presence of small amounts of cumulus/stratocumulus over the oceanic high center. The enhanced low-level cloud cover in the warm sector of the continental system could be due to the transport of moisture from the Gulf of Mexico by the southerly airstream.

The distribution of weather types associated with continental systems (Fig. 5c) is characterized by a higher frequency of light rain in the warm sector, and by a lower frequency of heavy snow in the cold sector when compared with the corresponding distribution for oceanic systems (Fig. 4c). There are also relatively more reports of fog in the land composite along the eastern edge of the precipitation zone. The locations of these fog observations correspond approximately to the United States eastern seaboard.

The location of precipitating weather in Fig. 5c is consistent with the distribution of vertical motion at 500 mb as inferred from the ECMWF analyses (see contours in the same panel). Comparison between the land composites for weather type (Fig. 5c) and for cloud type (Fig. 5a) also reveals a slight eastward shift of the cloud shield from the precipitation zone. This spatial relationship has been noted in the maritime system (Fig. 4).

The most salient difference in the near-surface wind circulation accompanying the maritime and continental systems is the much stronger cross-isobaric component over land. This land–sea contrast is an indication of the more prominent role of friction over continental surfaces. The nature of the cross-isobaric flow is explored in greater detail in Fig. 6, which shows the composites

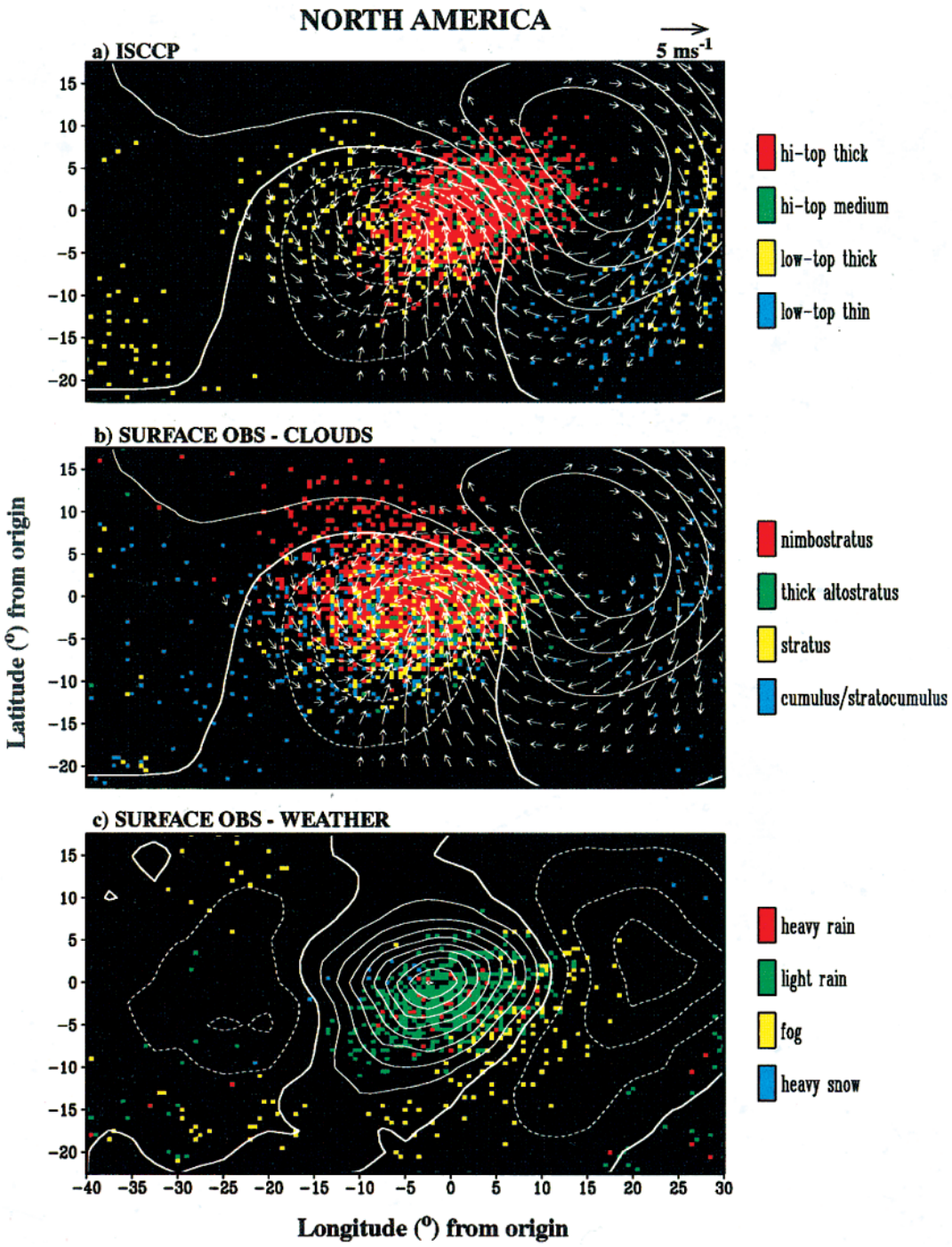

FIG. 5. As in Fig. 4 but based on 20 reference sites located in the eastern half of the North American continent.

of the geopotential height (contours), horizontal wind (arrows), and the angle (in degrees) between the actual wind vector and the geostrophic wind vector (stippling), all at the 1000-mb level. The results based on the combination of the 20 reference sites over the North Atlantic and North America are shown in Figs. 6a and 6b, respectively. For both the maritime and continental systems, the flow across the height contours is most notable to the west and northwest of the low center. The surface winds also exhibit a considerable cross-isobaric component in the region located at 10°–20° of latitude south of the low center. In the land composite, another area of strong ageostrophic flow is discernible just west of the high center. The angular deviation from geostrophy

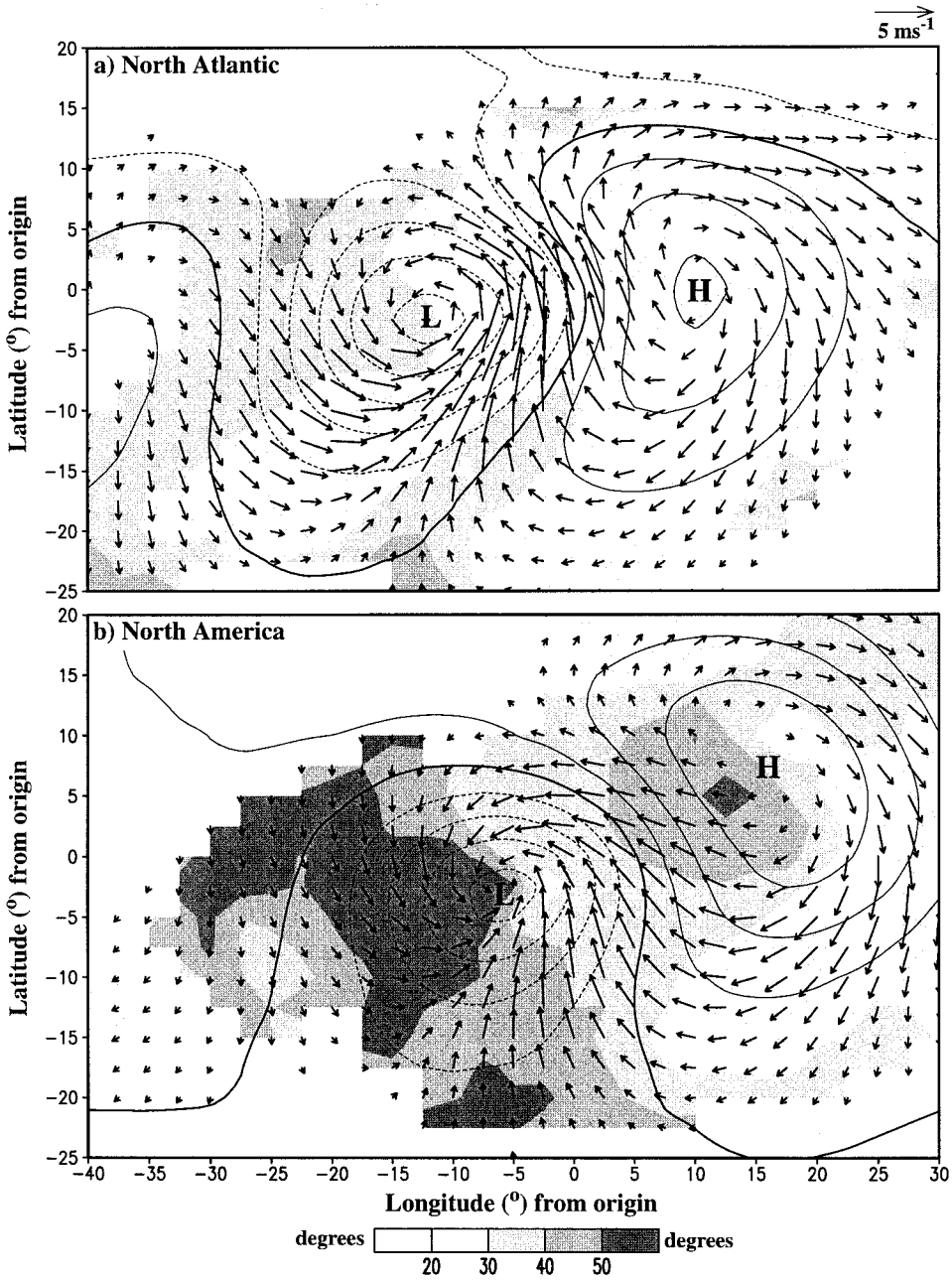

FIG. 6. Composite patterns of the anomalous horizontal wind (arrows, see scaling at top right) and geopotential height (contours, interval: 10 m) at 1000 mb, based on 20 reference sites in (a) North Atlantic and (b) eastern North American continent. Solid (dashed) contours indicate positive (negative) values. The angular deviation of the 1000-mb flow from the local geostrophic wind vector is indicated by stippling (see scale bar at bottom; units: degrees).

in the above areas is approximately 20°–30° over the North Atlantic and increases markedly to 40°–50° over North America. It is also noteworthy that the wind speeds in the vicinity of the oceanic low (Fig. 6a) are generally higher than those near the continental cyclone (Fig. 6b). In examining Fig. 6, it should be borne in mind that the ageostrophic characteristics presented therein may be somewhat dependent on the treatment of surface friction in the ECMWF models used for producing the wind and geopotential height analyses. An independent check of the ageostrophic features noted here could be performed by constructing analogous composites using actual wind and pressure observations taken at ships and surface stations.

The enhanced near-surface convergence associated with the strong cross-isobaric flow in the west-north-

western quadrant and the southern quadrant of the continental low pressure area may account for the more frequent occurrence of low-top thick or stratiform cloud cover in these sectors of the cyclones over land (see yellow pixels in Figs. 5a and 5b). As noted by Carlson (1991, Section 9.1), the extensive decks of low stratus clouds often seen to the northwest of midlatitude cyclones are associated with frictionally forced ascent in the boundary layer, and with dynamically forced descent (mostly due to negative temperature advection) at higher altitudes.

5. Cloud patterns accompanying tropical disturbances

To examine the cloud organization in prevalent tropical weather systems in the western Pacific, the composite procedure described in the previous sections has been applied to the cloud and ECMWF data in that region for the warm season (June through September). An array of 15 reference sites extending from 11° to 21°N, and from 121° to 141°E (see Fig. 5c of LC95) are used in determining the key dates for constructing the composites. The patterns for the anomalous amounts of selected cloud types, as obtained by combining the 15 individual composites in a common coordinate system, are shown using stippling in Fig. 7 for the ISCCP data (left panels) and the surface synoptic reports (right panels). Superposed on the cloud patterns are composites of the ECMWF data for height (contours) and wind (arrows) at 1000 mb.

The satellite composites are representative of the cloud organization in tropical convective disturbances. Some of these circulation systems are associated with the wavelike phenomena described by Lau and Lau (1990), among others. The cloudy episodes considered in the composite procedure may also include typhoon passages. In their typically northwestward journey across the western Pacific, the tropical wave and typhoon disturbances are accompanied by thick clouds with high tops in the vicinity of the low pressure center (see Fig. 7a). The deep convective towers thin out gradually toward the trailing edge of the system, so that the anvil-type clouds with high tops and relatively lower τ prevail to the south-southeast of the low center (Fig. 7b), where the outflow in the upper troposphere preferentially occurs. The leading edge of these systems (i.e., north of the low) is populated by low-top/thin cloud elements (Fig. 7c).

Comparison between Figs. 7a and 7d reveals that the high-top/thick clouds detected by the satellites are collocated with nimbostratus clouds as observed from the surface, thus suggesting that the cloud cover near the low center has a large vertical extent. The surface-based cloud type that exhibits the closest spatial correspondence to the high-top/thin clouds (Fig. 7b) is thin altostratus (Fig. 7e). In particular, note the enhanced cloud amounts south of the low center in Figs. 7b and 7e. A good match is evident between the enhanced cumulus (Fig. 7f) and low-top/thin (Fig. 7c) clouds at the northern (leading) edge of the system. In the region south of the low center, the cumulus clouds appearing in the surface-based composite (Fig. 7f) are not evident in the satellite composites for low-top/thin (Fig. 7c) clouds. These low clouds may be obscured from the satellite view by the high-top anvil clouds lying aloft.

The composites of the surface reports of nonprecipitating stratocumulus and stratus clouds (not shown) indicate an increase of more than 5% of these cloud types in the vicinity of the low center. These results are contrary to the reduction of cloudiness in that region, as inferred from the ISCCP composite of low-top/thick cloud, which has a pattern similar to Fig. 7c. The underestimation of low cloud amount in the satellite composite is again attributable to the shielding effect of the high-top/thick clouds above the low center (Fig. 7a).

The cloud types displayed separately in individual panels in Fig. 7 are combined in the color mosaics in Fig. 8a for ISCCP and Fig. 8b for surface data. The anomalous frequency of light rain and heavy rain reports is presented in Fig. 8c. Superposed on the pixel patterns are ECMWF products of anomalous 1000-mb height and wind in Figs. 8a and 8b, and 500-mb vertical velocity in Fig. 8c. The procedure for filling the color pixels is similar to that used in constructing Figs. 4 and 5 for the extratropical cyclones, except that each pixel in Fig. 8 represents a one-half percent enhancement of a certain cloud type or weather type.

The pattern in Fig. 8a illustrates more clearly the north–south asymmetry in the cloud-top altitude of the optically thin clouds with respect to the low center, with virtually all the low clouds being situated to the north, and the high clouds to the south. The low center itself is primarily covered by high-top/thick clouds. This organization is reproduced to a certain extent by the surface-based composite (Fig. 8b), which yields a relatively higher abundance of low-lying cumulus clouds underneath the anvil clouds situated south of the low center.

The composite of weather types (Fig. 8c) indicates the occurrence of heavy and light rain through much of the low center. The broad pattern of precipitation based on surface observations is in good agreement with the shield by high-top/thick clouds as deduced independently by the satellite dataset (Fig. 8a). The precipitation zone is also consistent with the region of ascent inferred from the ECMWF analyses. The extension of heavy rain to the southeast of the low center may be related to the enhanced divergent outflow at 200 mb in this quadrant (see Fig. 10c of LC95). The number of rain reports is much less in the regions of weak subsidence located near the northern and southern edges of the plotting domain.

6. Discussion

Previous studies on the relationships between cloud cover and atmospheric flow patterns are often based on

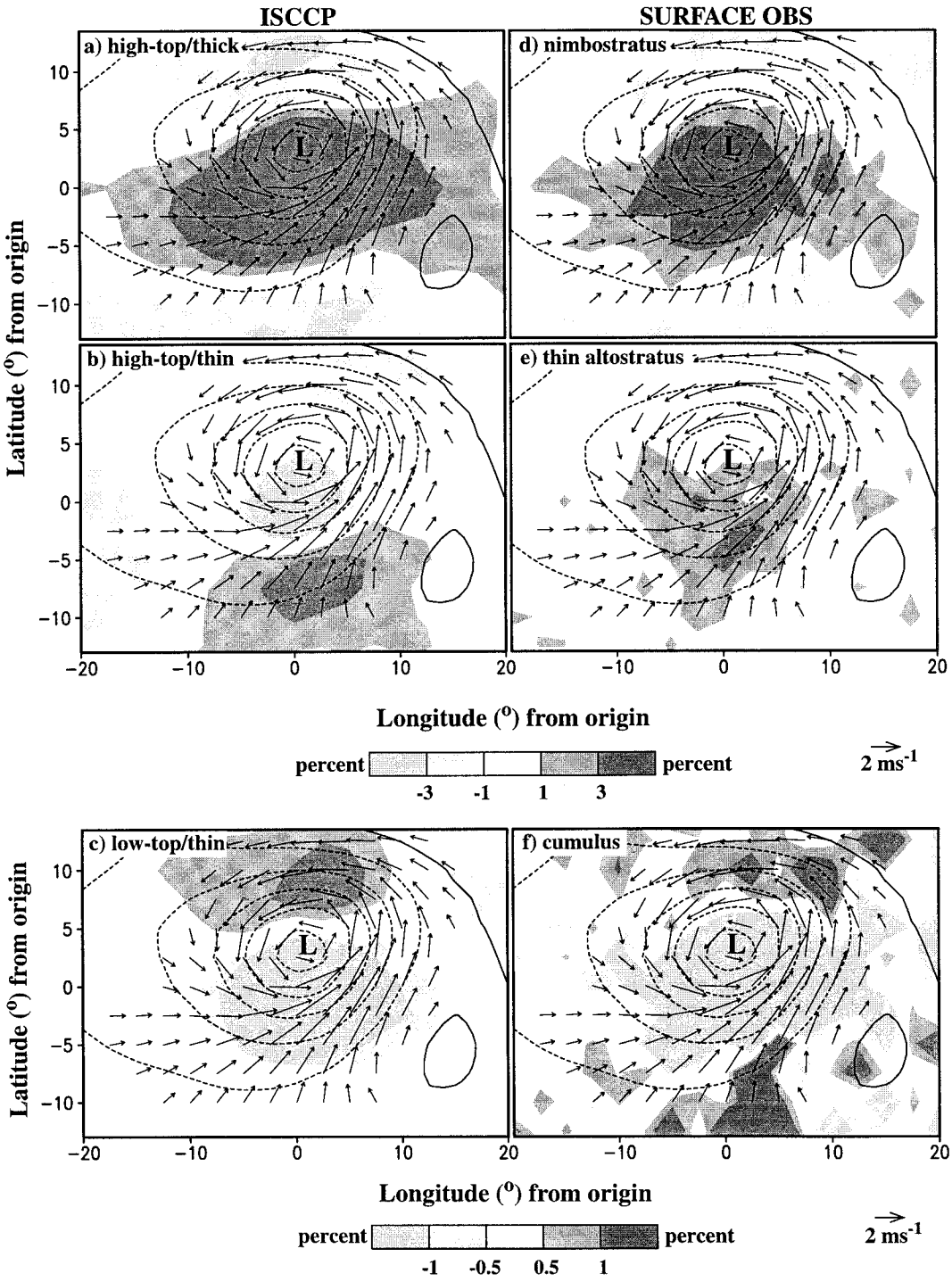

FIG. 7. As in Fig. 3 but for composite patterns based on 15 reference sites in the subtropical western Pacific, and for (a) high-top/thick, (b) high-top/thin, and (c) low-top/thin clouds in the ISCCP dataset, and (d) nimbostratus, (e) thin altostratus, and (f) cumulus in the surface reports. Note the different scale bars used for the top four panels and for the bottom two panels. Contour interval for anomalous 1000-mb height field: 5 m. Solid (dashed) contours indicate positive (negative) values.

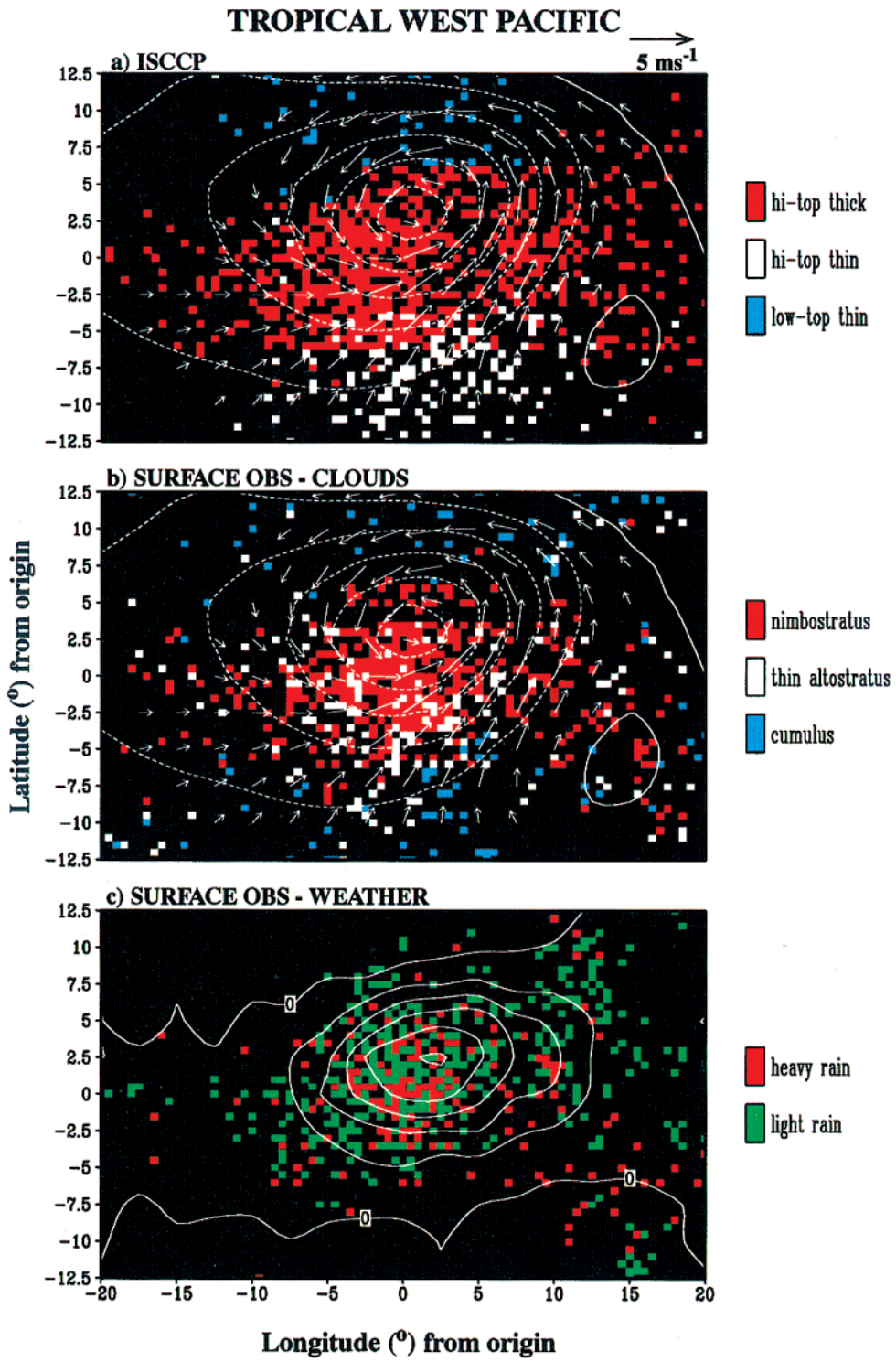

FIG. 8. As in Fig. 4 but for composite patterns based on 15 reference sites in the subtropical western Pacific. Each color represents 0.5% increment in cloud amount or frequency of occurrence of weather types. Contour intervals for anomalous 1000-mb height and vertical velocity fields: 5 m and 2×10^{-2} Pa s^{-1}. Solid (dashed) contours indicate positive (negative) values.

qualitative interpretations of the pertinent data fields. Comparisons between satellite and surface observations of cloudiness have heretofore mostly been concerned with climatological statistics. In LC95 and the present paper, special analysis tools have been designed to investigate the interactions between the cloud and circulation fields on a more quantitative and objective basis, and to compare in greater detail the satellite- and surface-based cloud patterns associated with two specific synoptic phenomena: the midlatitude cyclone wave, and the tropical convective disturbance. An overall consistency is noted between the propagation characteristics and spatial structure of cloud cover as deduced from the ISCCP products and the corresponding results obtained using surface observations. This general agreement among the two sets of findings lends credibility to the usefulness of both datasets for diagnosing a wide range of atmospheric behavior. It is demonstrated that the complementary nature of the two datasets, with the satellite platforms viewing the top of the cloud systems from space and the surface observers examining the same systems from below, can provide useful information on the vertical distribution of cloudiness. Several discrepancies are noted between the results based on ISCCP and surface observations. The most striking example is the underrepresentation in the satellite composite of low-level clouds under the high cloud shield east of the extratropical cyclone center (compare Figs. 3c and 3g). Some of these differences are evidently attributable to systematic biases inherent in the observing techniques and data processing procedures used in producing the datasets examined here.

The ISCCP and surface cloud observations have been collected using radically different methodologies. Moreover, the amount of various cloud types in these two datasets has been defined by applying disparate sampling procedures in both the spatial and temporal domains. Implicit in such definitions and data reduction procedures are many assumptions concerning the characteristic space scales and timescales for space and surface observations. For instance, the ISCCP estimates of the cloud amounts are based on sampling within a 3-h window of satellite pixels situated in square grid boxes with dimensions of 280 km, whereas the cloud amounts entered into an individual surface synoptic report pertain to the instantaneous skycover within the field of view of the observer (typically limited to tens of kilometers). Inspite of the dissimilarities among the information input from satellite and surface observations, some degree of consistency among the results based on these two datasets is still discernible. This level of agreement between the findings from the two data sources is achieved in part by incorporating a large number of similar events in the composite procedure.

Pursuant to the demonstration of the applicability of satellite and surface cloud data products to the study of selected circulation systems and the attendant atmospheric processes, it may be of interest to analyze the interactions among the cloud and circulation fields in other meteorological features. The scope of these investigations could conceivably be extended beyond the midlatitude cyclones and tropical disturbances considered thus far to phenomena with a broad range of space scales and timescales. Such circulation systems could include mesoscale features in extratropical frontal zones and low-latitude convective complexes, marine stratus decks associated with subtropical anticyclones, propagating intraseasonal oscillations near the equator, teleconnection patterns in the monthly and seasonal averaged midlatitude flow, and variations related to the El Niño–Southern Oscillation. Some of the above phenomena (such as those related to mesoscale processes) would have to be examined using cloud and other meteorological data with high spatial and temporal resolutions (on the order of 10–30 km and several hours, respectively). New analysis procedures would have to be developed for examining specific classes of phenomena. For instance, individual case studies (instead of composite analysis) are probably more suited for investigating the nature of subsynoptic cloud features. Sustained efforts to examine different modes of atmospheric variability by the joint application of satellite cloud products and conventional meteorological datasets (such as wind, temperature, and geopotential height fields) will hopefully facilitate closer interactions among the research communities specializing in atmospheric dynamics and those in cloud and radiation processes.

Acknowledgments. We thank J. R. Norris for making the surface synoptic reports available to us, S. A. Klein and J. M. Wallace for helpful discussions in the research phase of this work, and A. J. Broccoli, A. D. Del Genio, S. A. Klein, J. R. Lanzante, J. R. Norris, and B. J. Soden for offering perceptive comments on the manuscript.

APPENDIX

Data Analysis Procedures

The surface reports are first sorted according to time and location of observation. For a given day, surface observations taken within individual grid boxes with dimensions of 2.5° of latitude by 2.5° of longitude are grouped together. This particular size of the grid boxes has been chosen to match the spatial resolution of the ISCCP and ECMWF datasets. At each grid box, a daily tally is then taken of the available number of reports N_{ct} of each selected cloud type ct and of the available number of reports N_{wt} of each selected surface weather type wt.

The cloud types ct processed in this study include cumulus (Cu), stratocumulus (Sc), stratus (St), cumulonimbus (Cb), fog (Fg), thin and thick altostratus (As), thin and thick altocumulus (Ac), nimbostratus (Ns), thin and thick cirrus (Ci), cirrostratus (Cs), cirrocumulus (Cc), and a special category indicating the total cloud

cover. The definitions of these cloud types in terms of the standard synoptic codes are given in Table 2 of Hahn et al. (1994). These individual cloud types are grouped into three broad cloud levels cl according to the altitude of the cloud base: Cu, Sc, St, Cb, and Fg are classified as low clouds; As, Ac, and Ns are regarded as middle clouds; and Ci, Cs, and Cc are treated as high clouds.

Several broad categories of weather types wt are considered in this study: heavy rain [corresponding to reports with standard World Meteorological Organization weather codes (ww) indicating values of 63–65 and 81–82], light rain (ww = 14–16, 20–21, 25, 50–55, 58–62, and 80), heavy snow (ww = 37, 39, 73–75, and 86), light snow (ww = 22, 26, 36, 38, 70–72, 76–79, 85), and fog (ww = 10–12, 28, and 40–49). This grouping is coarser than that used by Petty (1995), who partitioned the weather codes according to intensity (extremely light, light, moderate/heavy, etc.), phase (liquid, snow, mixed, hail, etc.), and character (steady, showery, strong convection, etc.) of the precipitation being reported. Almost all weather codes contributing to light precipitation (rain or snow) in our study are assigned to the light or extremely light intensity classes by Petty. Similarly, heavy precipitation in our study corresponds well to the moderate/heavy intensity class in Petty's scheme. The snow and liquid categories used in the two classification methods are also consistent with each other.

A separate daily tally is taken of the total number of contributing reports $N^{\mathrm{cl}}_{\mathrm{total}}$ for each of the three cloud levels cl, and of the total number of surface weather observations N^{w}_{total}. Note that $N^{\mathrm{cl}}_{\mathrm{total}}$ represents a count of all available observations (including reports of clear sky) for a given cloud level. It is possible that a given synoptic report contributes to $N^{\mathrm{cl}}_{\mathrm{total}}$ at a certain cloud level but not to the tally at other levels. The daily sum of the N_{ct} observations of fractional cover F_{ct} by each selected cloud type ct, that is, $\overline{F_{\mathrm{ct}}} = \Sigma\, F_{\mathrm{ct}}$, is also stored in each grid box. Here the summation is taken over the available N_{ct} observations for a given day. The quantity $\overline{F_{\mathrm{ct}}}$, when divided by N_{ct} represents the daily averaged fractional cover at a given grid box by cloud type ct when it is present. This variable, $\overline{F_{\mathrm{ct}}}$, will be used in Eq. (A1) to define the cloud amount.

The end product of the data processing procedure described above consists of daily time series of gridded, near-global arrays of $\overline{F_{\mathrm{ct}}}$, N_{ct}, N_{wt}, $N^{\mathrm{cl}}_{\mathrm{total}}$, and N^{w}_{total} for each cloud or weather type, and for each cloud level. These arrays portray the spatial distributions of the occurrence of individual cloud or weather categories during a specific day, and are hence suited for mapping or diagnosis using various techniques developed for conventional meteorological fields. Inspection of the data coverage over our regions of interest (i.e., the northwestern sector of the tropical Pacific and midlatitude Northern Hemisphere) indicates that the average number of contributing synoptic low-cloud (middle-cloud) reports in a 2.5° × 2.5° grid box ranges from 1–2 (0.5–1) per day in the tropical and extratropical maritime sites, to 4–6 (3–4) per day in the extratropical land sites.

Following Hahn et al. (1994), the climatological amount $\mathrm{CLIM}_{\mathrm{ct}}$ of a given cloud type ct in a given grid box is obtained by

$$\mathrm{CLIM}_{\mathrm{ct}} = \frac{\sum N_{\mathrm{ct}}}{\sum N^{\mathrm{cl}}_{\mathrm{total}}} \frac{\sum \overline{F_{\mathrm{ct}}}}{\sum N_{\mathrm{ct}}}. \tag{A1}$$

Here all summations are taken over all the days in either the 6-month northern cool season (October through March) or the 4-month northern warm season (June through September) within the 1983–90 period. This specific period is chosen to match the temporal coverage of the ISCCP dataset used in LC95. The superscript cl in the term $N^{\mathrm{cl}}_{\mathrm{total}}$ in Eq. (A1) indicates the cloud level category under which the cloud type ct in question is classified (see details earlier in this appendix). For instance, $N^{\mathrm{cl}}_{\mathrm{total}}$ for low clouds is used to determine the climatology of stratus, whereas $N^{\mathrm{cl}}_{\mathrm{total}}$ for middle clouds is used to compute the corresponding statistic for altostratus.

The definition in Eq. (A1) may be interpreted as follows. Since $N^{\mathrm{cl}}_{\mathrm{total}}$ represents the number of contributing reports of cloudiness at level cl, the ratio $\Sigma N_{\mathrm{ct}}/\Sigma N^{\mathrm{cl}}_{\mathrm{total}}$ [first fraction on the rhs of Eq. (A1)] is hence a measure of the mean frequency of the occurrence of cloud type ct. Also recalling that $\overline{F_{\mathrm{ct}}}$ is the sum of fractional cloud cover reported in N_{ct} observations in a given day, the fraction $\Sigma\, \overline{F_{\mathrm{ct}}}/\Sigma\, N_{\mathrm{ct}}$ [second fraction on the rhs of Eq. (A1)] thus represents the long-term averaged fraction of coverage by ct when it is present. The climatological cloud amount is, therefore, seen to be the product of the mean frequency of a given cloud type and the mean fractional cover by this cloud type when it occurs.

In analogy with the definition for frequencies of individual cloud types, the climatological frequency of the occurrence of a given weather type wt in a grid box is computed as

$$\mathrm{CLIM}_{\mathrm{wt}} = \frac{\sum N_{\mathrm{wt}}}{\sum N^{w}_{\mathrm{total}}}. \tag{A2}$$

To ensure that the cloud- or weather-type climatologies are based on sufficient data input, the above computations are performed only for grid boxes where $N^{\mathrm{cl}}_{\mathrm{total}}$ or N^{w}_{total} are nonzero in at least 25% of the total number of days in seven seasons considered here. The climatology is regarded as missing for grid boxes that fail to meet this criterion and no further analysis is made for these boxes.

The typical cloud and weather patterns accompanying selected synoptic episodes are described using a composite procedure. Suppose that altogether M outstanding synoptic cases are identified, then the composite amount $\mathrm{COMP}_{\mathrm{ct}}$ of the cloud type ct and the composite frequency $\mathrm{COMP}_{\mathrm{wt}}$ of the weather type wt in each grid box can be computed using formulae analogous to those in Eq. (A1) and (A2), except that all summations are

taken over the common set of M cases only (instead of every day of a certain season in all years considered, as is done in evaluating the climatology). The composite values for a given grid box are determined only if $N^{\text{cl}}_{\text{total}}$ or N^{w}_{total} are nonzero in at least 25% of the M selected cases. Otherwise the composite cloud amount or weather type is treated as missing for the grid box in question. The departures of the composite data from the long-term climatology are represented by the anomalies $\text{ANOM}_{\text{ct}} = \text{COMP}_{\text{ct}} - \text{CLIM}_{\text{ct}}$ and $\text{ANOM}_{\text{wt}} = \text{COMP}_{\text{wt}} - \text{CLIM}_{\text{wt}}$.

REFERENCES

Blackmon, M. L., 1976: A climatological spectral study of the 500-mb geopotential height of the northern hemisphere. *J. Atmos. Sci.,* **33,** 1607–1623.

——, J. M. Wallace, N.-C. Lau, and S. L. Mullen, 1977: An observational study of the Northern Hemisphere wintertime circulation. *J. Atmos. Sci.,* **34,** 1040–1053.

——, Y.-H. Lee, J. M. Wallace, and H.-H. Hsu, 1984: Time variation of 500-mb height fluctuations with long, intermediate, and short time scales as deduced from lag-correlation statistics. *J. Atmos. Sci.,* **41,** 981–991.

Carlson, T. N., 1991: *Mid-Latitude Weather Systems.* Harper Collins, 507 pp.

Hahn, C. J., S. G. Warren, and J. London, 1994: Edited synoptic cloud reports from ships and land stations over the globe, 1982–1991. Carbon Dioxide Information Analysis Center Rep. NDP026B, 47 pp. [Available from Data Support Section, National Center for Atmospheric Research, P.O. Box 3000, Boulder, CO 80307.]

Holloway, J. L., Jr., 1958: Smoothing and filtering of time series and space fields. *Advances in Geophysics,* Vol. 4, Academic Press, 351–389.

Lau, K.-H., and N.-C. Lau, 1990: Observed structure and propagation characteristics of tropical summertime synoptic scale disturbances. *Mon. Wea. Rev.,* **118,** 1888–1913.

Lau, N.-C., 1979: The observed structure of tropospheric stationary waves and the local balances of vorticity and heat. *J. Atmos. Sci.,* **36,** 996–1016.

——, and M. W. Crane, 1995: A satellite view of the synoptic-scale organization of cloud properties in midlatitude and tropical circulation systems. *Mon. Wea. Rev.,* **123,** 1984–2006.

Petty, G. W., 1995: Frequencies and characteristics of global oceanic precipitation from shipboard present-weather reports. *Bull. Amer. Meteor. Soc.,* **76,** 1593–1616.

Rossow, W. B., and R. A. Schiffer, 1991: ISCCP cloud data products. *Bull. Amer. Meteor. Soc.,* **72,** 2–20.

Schiffer, R. A., and W. B. Rossow, 1983: The International Satellite Cloud Climatology Project (ISCCP): The first project of the World Climate Research Program. *Bull. Amer. Meteor. Soc.,* **64,** 779–784.

Trenberth, K. E., 1992: Global analyses from ECMWF and atlas of 1000 to 10 mb circulation statistics. NCAR Tech. Note NCAR/TN-373+STR, 191 pp. [Available from Information Services, National Center for Atmospheric Research, P.O. Box 3000, Boulder, CO 80307.]

Wallace, J. M., G.-H. Lim, and M.L. Blackmon, 1988: Relationship between cyclone tracks, anticyclone tracks, and baroclinic waveguides. *J. Atmos. Sci.,* **45,** 439–462.

Warren, S. G., C. J. Hahn, J. London, R. M. Chervin, and R. L. Jenne, 1986: Global distribution of total cloud and cloud type amounts over land. NCAR Tech. Note NCAR/TN-273+STR/DOE Tech. Rep. ER/60085-HI, 29 pp. + 200 maps. [NTIS DE87-00-6903.]

——, ——, ——, ——, and ——, 1988: Global distribution of total cloud and cloud type amounts over the ocean. NCAR Tech. Note NCAR/TN-317+STR/DOE Tech. Rep. ER-0406, 42 pp. + 170 maps. [NTIS DE90-00-3187.]